Molecular Crystals and Liquid Crystals

Publication details, including instructions for authors and subscription information:
http://www.tandfonline.com/loi/gmcl20

Linear and Nonlinear Optics of Confined Chiral Liquid Crystals at Weak Surface Anchoring

V. A. Belyakov [a]

[a] L. D. Landau Institute for Theoretical Physics, Moscow, Russia

Version of record first published: 22 Sep 2010

To cite this article: V. A. Belyakov (2007): Linear and Nonlinear Optics of Confined Chiral Liquid Crystals at Weak Surface Anchoring, Molecular Crystals and Liquid Crystals, 467:1, 155-169

To link to this article: http://dx.doi.org/10.1080/15421400701221385

Mol. Cryst. Liq. Cryst., Vol. 467, pp. 155–169, 2007

ISSN: 1542-1406 print/1563-5287 online
DOI: 10.1080/15421400701221385

Taylor & Francis
Taylor & Francis Group

Linear and Nonlinear Optics of Confined Chiral Liquid Crystals at Weak Surface Anchoring

V. A. Belyakov
L. D. Landau Institute for Theoretical Physics, Moscow, Russia

The theoretical description of the optical properties of confined chiral liquid crystals (CLC) under action of a varying external agent for light propagating along the chiral axes is performed. The observed jumps and the hysteresis of the optical properties of confined CLC under action of a varying external agent are related to the surface anchoring. The detailed examination of the problem is carried out for the varying agent being the thickness of a planar layer in the case of a finite anchoring strength. Analytical expressions for the solution of the boundary-value problem for the absorbing (amplifying) CLC dependent on the layer thickness are presented. In particular, the equation for the lasing threshold for the edge lasing mode in a distributed feedback (DFB) lasing is obtained and analyzed. The connection of the optical characteristics of a CLC layer to the surface anchoring and, in particular, their discontinuity and hysteresis under variation of the layer thickness are demonstrated for a CLC layer of varying thickness and a wedge filled by CLC. It is shown that, in the case of a weak surface anchoring, the experimental measurements of the CLC layer optical characteristics under action of a varying external agent can be used to restore the actual surface anchoring potential.

Keywords: cano-granjean wedge; chiral LC; low threshold lasing; surface anchoring

INTRODUCTION

Unusual optical properties of chiral liquid crystals (CLC) attract now the new attention because these media are examples of photonic crystals of natural origin and due to the fact that the photonic crystals and, in particular, CLC promise numerous effective applications in linear and nonlinear optics. The exotic optical properties of CLC are understood since the pioneer work of De Vries [1] and are well described now within the analytical approach [2–4] and by numerical calculations based mainly

The work is supported by the RFBR grant 06-02-16287.
Address correspondence to V. A. Belyakov, L. D. Landau Institute for Theoretical Physics, 2, Kosygin Str., Moscow, 117334, Russia. E-mail: bel@landau.ac.ru

on the Berreman method [5]. However, it happens that the optics of confined CLC (in the simplest case, a plane CLC layer) reveals some features which demand a rather careful application of the developed approaches to the CLC optics if some varying external agents are applied to CLC. These varying agents may be the temperature, applied external field, mechanical twist, and so on. The experiment shows that, under the action of smoothly, continuously varying external agents, the optical properties of confined CLC vary smoothly in the limited range of the agent variations, and, at some values of agents, jump-like changes the optical properties occur. Moreover, there is a hysteresis of the optical properties if the direction of the agent variation is changed. The jumps and the hysteresis of the optical properties most clearly were observed at temperature variations [6]. Similar phenomena were observed also at a mechanical twist of the nematic layer [7] and in externally applied electric (magnetic) fields [8]. In nonlinear optics, the jumps and hysteresis reveal themselves in the nonlinear optical harmonic generation [9] and the distributed feedback (DFB) lasing in CLC [10].

The connection of the CLC layer optical characteristics and the hysteresis to the surface anchoring [11,12] are demonstrated below for a CLC layer of varying thickness and a wedge filled by CLC.

EIGENWAVES IN CHIRAL LC

Let us begin to describe the CLC optical properties from those of unlimited CLC. As known [1–4], the eigenwaves corresponding to the propagation of light in chiral LC along a spiral axis are presented by a superposition of two plane waves of the form

$$\mathbf{E}(z,t) = e^{-i\omega t}[\mathbf{E}^{+}\mathbf{n}_{+}\exp(i\mathbf{K}^{+}\mathbf{z}) + \mathbf{E}^{-}\mathbf{n}_{-}\exp(i\mathbf{K}^{-}\mathbf{z})], \tag{1}$$

where ω is the light frequency, $\mathbf{n}_{\pm}$ are two vectors of circular polarizations and the wave vectors $\mathbf{K}^{\pm}$ satisfy the condition

$$\mathbf{K}^{+} - \mathbf{K}^{-} = \boldsymbol{\tau}, \tag{2}$$

where $\boldsymbol{\tau}$ is the reciprocal lattice vector of the LC spiral.

The wave vectors $\mathbf{K}^{\pm}$ in four eigensolutions (1) are determined by Equation (2) and the formulas

$$\mathbf{K}_{j}^{+} = \tau/2 \pm \kappa\left\{1 + (\tau/2\kappa)^2 \pm [(\tau/\kappa)^2 + \delta^2]^{1/2}\right\}^{1/2}, \tag{3}$$

where j enumerates the eigensolutions with the ratio of amplitudes (E^{-}/E^{+}) given by the expression

$$(E^{-}/E^{+})_{j} = \delta/[(\mathbf{K}_{j}^{+} - \tau)^2/\kappa^2 - 1]. \tag{4}$$

Here, $\kappa = \omega\varepsilon_0{}^{1/2}/c$, $\varepsilon_0 = (\varepsilon_\| + \varepsilon_\perp)/2$, $\delta = (\varepsilon_\| - \varepsilon_\perp)/(\varepsilon_\| + \varepsilon_\perp)$ is the dielectric anisotropy, and $\varepsilon_\|$, $\varepsilon_\perp$ are the principal values of the LC dielectric tensor [2–4]. Two of the eigenwaves corresponding to the circular polarization with the sense of chirality coinciding with the one of the LC spiral experience the strong diffraction scattering at the frequencies in the region of the stop band. Because, as we shall see, the specificity of the CLC optics is connected with the eigenwaves of diffracting polarization, we limit ourselves below by consideration of the propagation and lasing of light of the diffracting polarization only in LC.

BOUNDARY-VALUE PROBLEM

To investigate the optics of confined CLC, we have to consider a boundary-value problem. We assume that the CLC is presented by a planar layer with a spiral axis perpendicular to the layer surfaces. We assume also that the average dielectric constant of the LC, $\square 0$, coincides with the dielectric constant of the external medium.

Begin the consideration of the boundary-value problem in the formulation which assumes that two plane wave of the diffracting polarization and of the same frequency are incident along the spiral axes at the layer from the opposite sides, and the dielectric tensor may have nonzero imaginary part of any sign. The amplitudes of the eigenwaves $E^+{}_j$ excited in the layer by the incident waves are determined by the equations [3,4]:

$$\begin{aligned} &(1 + \mathrm{K}_+^+/\kappa)E_+^+ + (1 + \mathrm{K}_-^+/\kappa)E_-^+ = 2E_{ir}, \\ &\exp[\mathrm{i}\ \mathrm{K}_+^+\mathrm{L}](1 - \mathrm{K}_+^+/\kappa)\mathrm{E}_+^+ + \exp[\mathrm{i}\ \mathrm{K}_-^+\mathrm{L}](1 - \mathrm{K}_-^+/\kappa)E_-^+ = 2E_{\mathrm{il}} \end{aligned}, \tag{5}$$

where E_{ir} and E_{il} are the amplitudes of the waves incident at the layer from the right and left sides, respectively, L is the layer thickness, and

$$\mathbf{K}_\pm^+ = \tau/2 \pm \kappa\{1 + (\tau/2\kappa)^2 - [(\tau/\kappa)^2 + \delta^2]^{1/2}\}^{1/2}. \tag{6}$$

The amplitudes of the waves leaving the layer from the right, E_{er}, and left, E_{el}, sides, respectively, are determined by the expressions

$$\begin{aligned} 2E_{\mathrm{er}} =& \{\delta/[(\mathrm{K}_+^+ - \tau)^2/\kappa^2 - 1]\} \\ &\times (1 - \mathrm{K}_+^+/\kappa)E_+^+ + \{\delta/[(\mathrm{K}_-^+ - \tau)^2/\kappa^2 - 1]\}(1 - \mathrm{K}_-^+/\kappa)E_-^+, \\ 2E_{\mathrm{el}} =& \exp[\mathrm{i}(\mathrm{K}_+^+ - \kappa)\mathrm{L}](1 - \mathrm{K}_+^+/\kappa)E_+^+ + \exp[\mathrm{i}(\mathrm{K}_-^+ - \kappa)\mathrm{L}] \\ &\times (1 - \mathrm{K}_-^+/\kappa)E_-^+. \end{aligned} \tag{7}$$

If one assumes that the amplitude of only one incident wave is nonzero, Equation (7) determines the reflected and transmitted waves (the reflection R and transmission T coefficients of the layer) and, in particular, their frequency dependence [3,4]. The corresponding expressions for R and T take the form

$$R = \delta^2|\mathrm{sinqL}|^2/|(\mathrm{q}\tau/\kappa^2)\mathrm{cosqL} + \mathrm{i}[(\tau/2\kappa)^2 + (\mathrm{q}/\kappa)^2 - 1]\mathrm{sinqL}|^2,$$
$$T = |\exp[\mathrm{i}\kappa\mathrm{L}](\mathrm{q}\tau/\kappa^2)|^2/|(\mathrm{q}\tau/\kappa^2)\mathrm{cosqL} + \mathrm{i}[(\tau/2\kappa)^2 + (\mathrm{q}/\kappa)^2 - 1]\mathrm{sinqL}|^2, \tag{8}$$

where

$$\mathrm{q} = \kappa\{1 + (\tau/2\kappa)^2 - [(\tau/\kappa)^2 + \delta^2]^{1/2}\}^{1/2}. \tag{9}$$

If the both amplitudes of the incident waves are equal to zero, no waves emerging from the layer exist if the dielectric tensor has a positive (or a very small negative) imaginary part.

ABSORBING LC

Examine the formulas of the previous section for absorbing CLC in more details. Assume for simplicity that the absorption in LC is isotropic. Define the ratio of the dielectric constant imaginary part to the real part of ε as γ, i.e. $\varepsilon = \varepsilon_0(1 + \mathrm{i}\gamma)$. We note that, in the real situations, $\gamma \ll 1$. In Figure 1, we present R and 1-R-T calculated versus the frequency for two positive values of γ and its zero value. As one can see from Figures 1, *b,c*, the absorption in the layer reaches maxima at some frequencies close to the stop band edge. Comparing the positions of these maxima with the positions of zero R in the reflection by a nonabsorbing layer, one sees that the corresponding positions are close. The enhanced absorption is a manifestation of the so-called effect of anomalously strong absorption [3,13].

Due to the assumed isotropy of the absorption, the frequency dependences of the calculated characteristics are symmetric relative to the Bragg frequency (the mid-point of the stop band). Therefore, only the frequencies above the Bragg frequency are presented in the figures. All above-mentioned quantities reveal the beats as functions of the frequency which are close to the frequency edge of the selective reflection band. The positions of corresponding maxima and minima are determined by the layer thickness L and δ and are slightly dependent on the value of γ. In absorbing LC, the sum of the intensities of the reflected and transmitted beams is less than the intensity of the incident beam, i.e., $R + T < 1$.

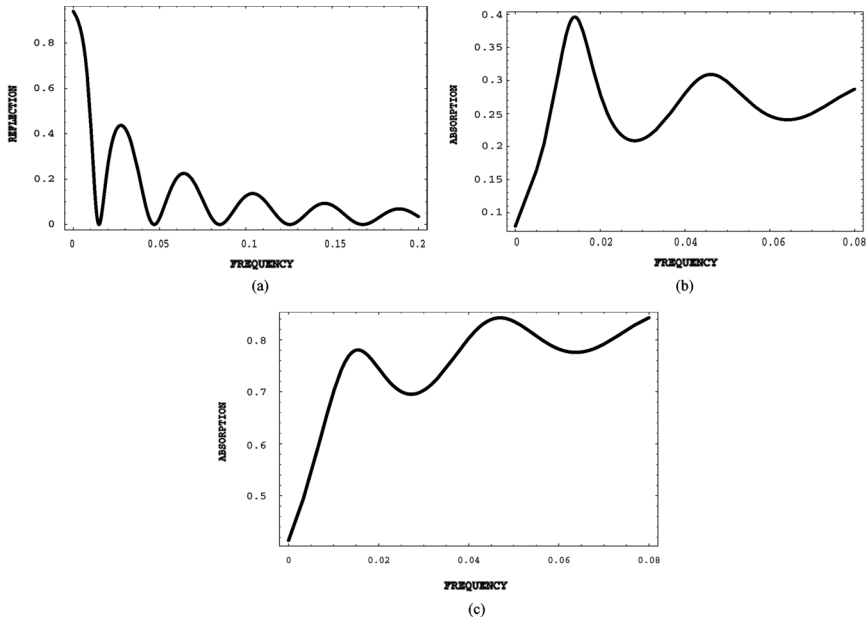

FIGURE 1 Calculated reflection R (a) for a nonabsorbing layer ($\gamma = 0$) and absorption ($1 - R - T$) versus the frequency measured from the stop band edge ($\nu = 2(\omega - \omega_B)/\delta\omega_B - 1$, $l = 300$, $l = L\tau$) (b) for $\gamma = 0.001$, (c) $\gamma = 0.005$.

As an example, the positions of the minima of beats of the reflection coefficient R (following from (8)) are given below for nonabsorbing LC, i.e., for $\gamma = 0$:

$$\begin{aligned} &qL = \pi n, \qquad \pm\nu = 1 + (\pi n/a)^2/2, \quad n = 1,\ 2,\ 3,\ \ldots \\ &\nu = 2(\omega - \omega_B)/\delta\omega_B, \quad \omega_B = c\tau/2\varepsilon_0^{1/2}, \quad a = \delta L\tau/4. \end{aligned} \tag{10}$$

In a typical situation, $a \gg 1$.

The edges of the selective reflection band ω_e are connected to the Bragg frequency ω_B by the relation

$$\omega_e = \omega_B/(1 \pm \delta)^{1/2} = c\tau/2[\varepsilon_0(1 \pm \delta)]^{1/2}. \tag{11}$$

So, at the edges, $\nu = 2(1/(1 \pm \delta)^{1/2} - 1)/\delta$.

For small γ and $L\mathrm{Im}q \ll 1$, the reflection and transmission coefficients (8) at the frequencies of the reflection minima (11) are reduced to the following expressions:

$$R = (a^3\gamma)^2/[(n\pi)^2 + a^3\gamma]^2, \qquad T = (n\pi)^4/[(n\pi)^2 + a^3\gamma]^2. \tag{12}$$

It follows from (10,12) that, for each n, the maximal absorption, i.e., the maximal $1 - R - T$, occurs for $(n\pi)^2 = a^3\gamma$. This means that the maximal absorption occurs for a special relation between δ, γ, and L. If this relation, i.e., $(n\pi)^2 = a^3\gamma$, is fulfilled, then $R = 1/4$, $T = 1/4$ and $1 - R - T = 1/2$. Because of the assumed smallness of γ, this result corresponds to a strong enhancement of the absorption for weakly absorbing layers.

AMPLIFYING LC

Now let us assume that $\gamma < 0$, which means that the chiral LC is amplifying. If $|\gamma|$ is sufficiently small, the waves emerging from the layer according to (5)–(8) exist, at any rate, only in the presence of one external wave incident on the layer, and their amplitudes are determined by the solution of Equations (5) and (7). Now (see Fig. 3c) $R + T > 1$ or $1 - R - T < 0$, which just corresponds to the definition of amplifying medium.

However, if the imaginary part of the dielectric tensor, i.e., γ, reaches some critical negative value, the quantity $R + T$ diverges, and the amplitudes of waves emerging from the layer occur to be nonzero even for the zero amplitudes of incident waves. The corresponding value of γ relates to the beginning of the DFB lasing in the CLC layer and is called a lasing threshold value. This happens when the determinant of Equation (5) reaches zero. The corresponding frequencies determine the so-called edge lasing modes [14–16] and the corresponding threshold values of the gain, at which the lasing happens.

So, the equation determining the edge lasing modes (zero value of the determinant of Equation (5) or the denominator of expressions (8)) looks as

$$\mathrm{tgqL} = \mathrm{i}(\mathrm{q}\tau/\kappa^2)/[(\tau/2\kappa)^2 + (\mathrm{q}/\kappa)^2 - 1]. \tag{13}$$

In the general case, this equation has to be solved numerically. However, for a very small negative imaginary part of the dielectric tensor, the threshold values of the gain for the edge lasing modes may be presented by analytical expressions.

For small $|\gamma|$ and $\mathrm{L}|\mathrm{Imq}| \ll 1$, the reflection and transmission coefficients (8) at the frequencies of the reflection minima (10) are reduced again to formulas (12), but with negative γ.

So the R and T may be divergent now, and the points of the R and T divergence correspond to the edge lasing modes and determine the corresponding values of threshold γ, i.e., a minimum $|\gamma|$, at which the lasing happens for the n-th reflection minimum:

$$\gamma = -(n\pi)^2/a^3 = -(n\pi)^2/(\delta L\tau/4)^3. \tag{14}$$

As one sees from (14), the threshold values of $|\gamma|$ are inversely proportional to the third power of the layer thickness, and the minimal value of $|\gamma|$ corresponds to $n = 1$, i.e., to the edge lasing mode closest to the selective reflection band edge. The calculated reflection and transmission intensities close to the frequencies of the first and second lasing modes are presented at Figure 2. In the calculations, it was accepted that the different threshold values of γ in Figure 2 corresponding to the different edge lasing modes (divergent R and T in Fig. 2a–d) were obtained for all other parameters of the layer to be fixed. This means that one is able to excite separate lasing modes by changing the gain (γ). If the value of γ is between the consequent threshold values of γ for neighboring lasing modes, the lasing cannot be achieved, and the layer can reveal only amplifying properties (see Fig. 3a–c). This means that the changing of the pumping wave intensity allows one to achieve the lasing at individual lasing modes,

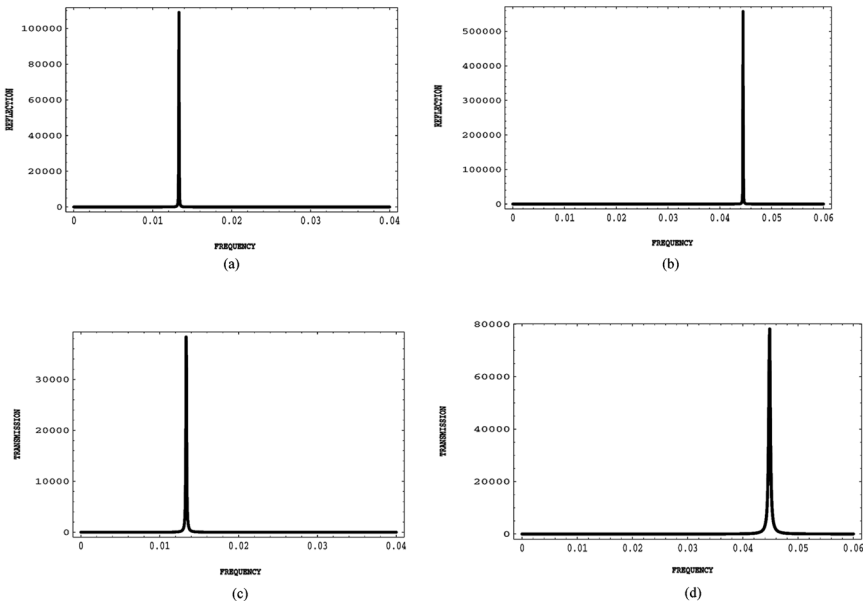

FIGURE 2 Calculated R versus the frequency ($\nu = 2(\omega - \omega_B)/\delta\omega_B - 1$, $l = 300$, $l = L\tau$) (a) close to the threshold gain for the first lasing edge mode ($\gamma = -0.00565$), (b) close to the threshold gain for the second lasing edge mode ($\gamma = -0.0129$); calculated T versus the frequency ($\nu = 2(\omega - \omega_B)/\delta\omega_B - 1$, $l = 300$, $l = L\tau$) (c) close to the threshold gain for the first lasing edge mode ($\gamma = -0.00565$), (d)) close to the threshold gain for the second lasing edge mode ($\gamma = -0.0129$).

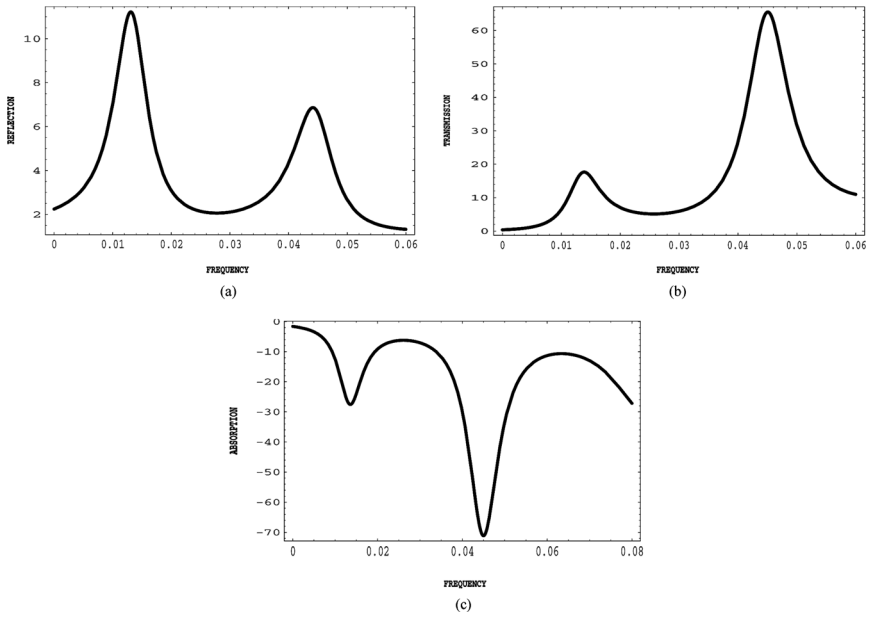

FIGURE 3 Calculated R (a), T (b), 1-R-T (c) versus the frequency ($\nu = 2(\omega - \omega_B)/\delta\omega_B - 1$, $l = 300$, $l = L\tau$) for $\gamma = -0.009$, i.e., for the gain between the thresholds for the first and second lasing edge modes.

and the lasing intensity is not a monotonic function of the pumping intensity. Sometimes, as the experiment shows, the smooth variations of an external agent can result in the jump-like variations of the lasing frequency [l0] connected with the jumps of a CLC pitch (see the next section) which are sensitive to the surface anchoring [12].

PLANE LAYER

The above-studied linear and nonlinear optical properties of a confined CLC vary smoothly only in the limited range of smoothly and continuously varying external agents. It is essential that, at some values of the agents, the jump-like changes of the optical properties occur. We now consider the CLC layer thickness as a varying external agent. Specifically, we will examine the behaviour of the cholesteric helix in a planar layer with a finite anchoring strength at one of its surfaces and the infinite anchoring one at the other surface. Assume that the alignment directions coincide at the both surfaces (see Fig. 4 considering the director deviation angle φ at one of the surfaces to be

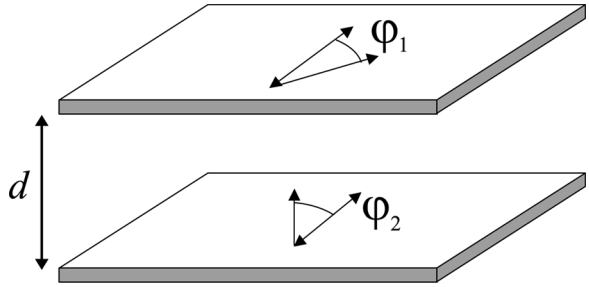

FIGURE 4 The case of nonidentical anchoring at the surfaces of a cholesteric layer (the line with two arrows indicates the easy direction).

identically equal to zero). We also assume, as in [6,11,17,18], that the pitch jump mechanism is connected with the director overcoming the anchoring barrier at the surface. The problem is similar to the problems related to the temperature- [6,11,17,19] and field-induced [18,20,21] variations of the director structure. Therefore, we recall here only the main equations describing the problem. The free energy of a homogeneous layer can be presented as

$$\mathbf{F}(\mathbf{T}) = \mathbf{W_s}(\varphi) + (\mathbf{K_{22}}/\mathbf{2d})[\varphi - \varphi_{\mathbf{0}}(\mathbf{d})]^{\mathbf{2}}, \tag{15}$$

where φ is the angle of the director deviation from the alignment direction at the surfaces with a finite anchoring, $\boldsymbol{W_s}(\varphi)$ is the surface anchoring potential, $\boldsymbol{K_{22}}$ is the elastic twist modulus, d is the layer thickness, the angle $\varphi_{\mathbf{0}}(\mathbf{d})$ gives the angle of the director deviation from the alignment direction at the surface with a finite anchoring if the anchoring at this surface were absent at all, i.e., $\varphi_{\mathbf{0}}(\boldsymbol{d}) = 2\pi d/p$, where p, or a natural pitch, is the value of a pitch in the bulk of a cholesteric LC.

One obtains the equation determining the angle φ at the surface of the layer as a function of d by minimization of Equation (15). The corresponding eqution is

$$\partial \mathbf{W_s}(\varphi)/\partial\varphi + (\mathbf{K_{22}}/\mathbf{d})(\varphi - \varphi_{\mathbf{0}}) = \mathbf{0} \tag{16}$$

Solving this equation for the different model anchoring potentials $\boldsymbol{W}_{\mathbf{s}}(\varphi)$ (see [22–25]), one finds that the angle φ, being a function of the thickness d, is also dependent on the dimensionless parameter $\boldsymbol{S}_{\mathbf{d}} = K_{22}/Wd$, where W is the depth of anchoring potential, and the specificity of its functional dependence on d and $\boldsymbol{S}_{\mathbf{d}}$ is different for the different model anchoring potentials [12,22–25]. Because $\boldsymbol{S}_{\mathbf{d}}$ is

variable in our problem, it is natural to introduce a new parameter which does not vary at variations of the layer thickness. It is convenient to introduce a new dimensionless parameter $l_p = L_p/p$, where $L_p = K_{22}/W$ is the so-called penetration length [2]. As a result, one gets the following form of Equation (16):

$$\partial \mathbf{W_s}(\varphi)/\partial\varphi + \mathrm{W}(\mathrm{S_d}\varphi - 2\pi \mathrm{l_p}) = 0. \tag{17}$$

The solution of Equations (16) and (17) is a smooth function of the thickness d (or the parameter S_d) in some ranges of the thickness d with abrupt jumps of φ at definite thicknesses of the layer, for which φ reaches the critical value φ_c. Just at these thicknesses, the linear and nonlinear optical characteristics of the CLC layer [see Eqs. (5)–(14)] experience jumps.

We investigate below the so-called B-potential recently introduced in [22–25] rather than the Rapini-Papoular (R-P) potential. Equation (18) for the B-potential is reduced to the form

$$\sin\varphi + 2\ \mathrm{S_d}\varphi - 4\pi \mathrm{l_p} = 0 \tag{18}$$

with the critical angle φ_c equal to $\pi/2$.

The solution of Equation (18) shows that, as φ achieves the critical value φ_c, both a jump-like change of the pitch and the transition to a new configuration of the helix differing by one in the number N of the director half-turns over the layer thickness occur.

The results of the numerical solution of Equation (18) for the B-potential are presented at Figures 5 and 6. Figure 5 presents the variations of the director half-turns in the layer versus the layer thickness for the increasing and decreasing layer thickness. The number N, along with smooth changes, reveals jumps at some points. Figure 6 presents an example of a possible hysteresis loop at the inversion of the direction of the layer thickness variation.

If the described jump happens in a limited area of the layer surface, the director distribution over the layer surface becomes inhomogeneous, and the wall (the interface between the configurations with N and $N+1$ half-turns of the director) occurs. The wall begins its motion in the direction of the N configuration, because the free energy of the N configuration per unit layer area is higher than the corresponding value for the $N+1$ configuration [23,24]. However, this wall may be motionless. This happens if the free energy of the N configuration per unit layer area is the same as the free energy for the $N+1$ configuration. In our case, these situations of the motionless walls take place at the thicknesses of the layer, for which $\varphi_0 = \pi/2$. At these points, the director at the layer surface with a finite anchoring makes

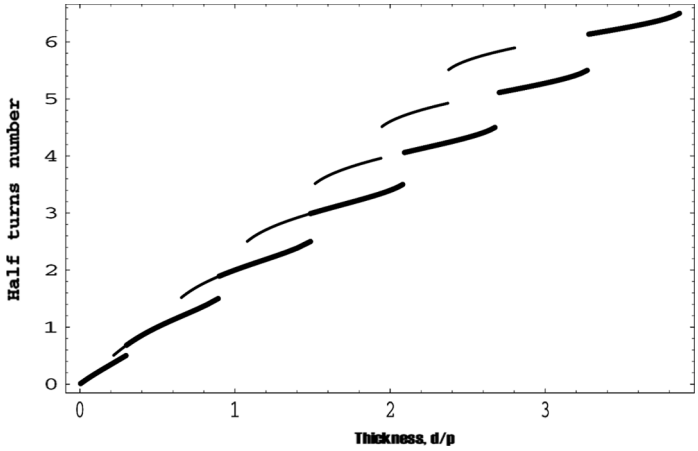

FIGURE 5 Change of the half-turns number in a plane layer versus the layer thickness (d/p) for the B-potential (the bold line at the increase of the thickness, and the narrow line at its decrease, $l_p = 0.5$).

the angles φ_e and $-\varphi_e$ relative to the alignment direction for the N and $N+1$ configuration, respectively. The jump of the director orientation at the layer surface is equal to $\pi - 2\varphi_e$, i.e., it is dependent on

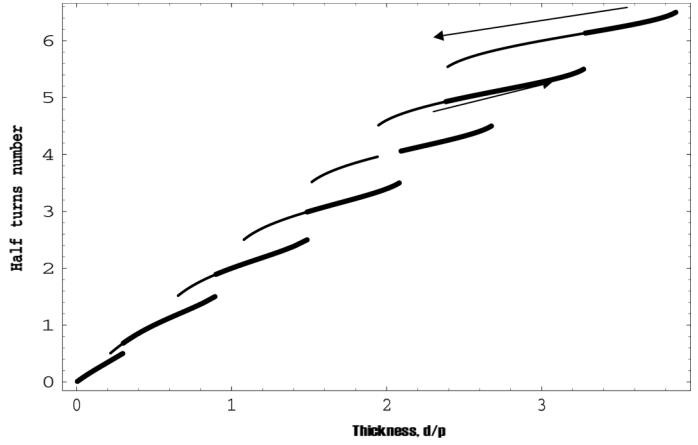

FIGURE 6 Hysteresis in the variation of the half-turns number in a plane layer versus the layer thickness (d/p) for the B-potential (the bold line at the increase of the thickness, and the narrow line at its decrease, $l_p = 0.5$) shown around $d/p = 3$ (The directions of the thickness variations are also shown by the arrows).

the layer thickness, at which the motionless wall exists. Relation (18) yields the equation for φ_e:

$$\sin \varphi_e + 2\, S_{de} \varphi_e - 4\pi l_p = 0. \tag{19}$$

Here, S_{de} is the value of S_d corresponding to the layer thickness, at which a motionless wall may exist. In our consideration, in which all parameters of the problem except the thickness d are fixed, a motionless wall exists for discrete thicknesses of the layer. One has to search for the solution of Equation (4) for the discrete values of S_d, i.e., for S_{de}. For this reason, the values of φ_e found from (19) are also discrete. The corresponding thicknesses of the layer d_e are determined by the expression

$$d_e/p = (2n + 1)/4, \tag{20}$$

where $n = 0,1,2,\ldots$ and p is the natural pitch of CLC.

WEDGE

The pitch variations in a plane layer versus the layer thickness can be directly measured in experiments. However, it seems that a wedge-shape sample gives a more easy way to do this. So, we will study how the behavior of the director configuration under variations of the planar layer thickness reveals itself in the Cano-Granjean wedge and its optical characteristics. We assume below that the wedge angle is small enough and the formulas obtained above for a planar layer of variable thickness may be applied locally to the wedge.

In a wedge, the director configurations just at the both sides of a Cano-Granjean line have to correspond to an equilibrium state of the system. For a such steady state, the free energies of the N and $N+1$ director configurations at the both sides of the wall have to be locally equal. This means that the walls in the wedge exist for the wedge thicknesses determined by Equation (20), so the parameters S_{de} and φ_0 in Equations (16) and (17) are known. Therefore, we have to calculate the smooth director reorientations at the surface between the two consecutive walls (the Cano-Granjean line) in the range determined by the consecutive values of d_e given by (20) for n and $n+1$. In a wedge, the jumps studied above for a layer are substituted by walls which can be non-singular for a sufficiently thin part of the wedge [24].

The results of calculations related to the dependence of the pitch on the local wedge thickness (d/p) in a wedge are presented at Figures 7 and 8 for the R-P and B anchoring model potentials, respectively. One

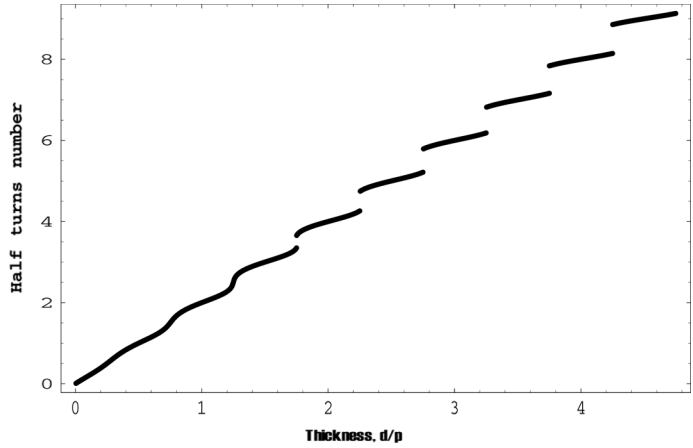

FIGURE 7 Variation of the half-turns number in a wedge versus the local wedge thickness (d/p) for the R-P-potential ($l_p = 1.5$).

sees a qualitative difference in the corresponding dependences for the R-P and B potentials at the thin part of the wedge. For the B-potential, the walls (pitch jumps) occur for any local thicknesses determined by Equation (20). But, for the R-P-potential, the walls (pitch jumps) at the thin part of the wedge can be absent and appear at a thickness d above some critical value. The walls for the R-P and B potentials reveal also differences in the shape of the director distribution over the wall and

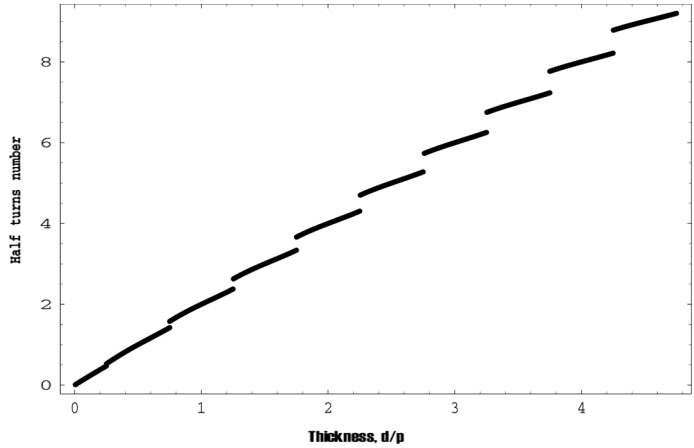

FIGURE 8 Variation of the half-turns number in the wedge versus the local wedge thickness (d/p) for the B-potential ($l_p = 1.5$).

the wall width [24], which have to be reflected in the optical wall images for the two surface anchoring model potentials.

CONCLUSION

The performed examination of the optics of confined CLCs under the action of a varying external agent shows that there is a direct connection between the surface anchoring and the CLC optical properties, and there are some phenomena in the field of interest for the CLC physics and for their numerous effective applications. As for the CLC physics, there are options to investigate the surface anchoring and, in particular, to restore the actual surface anchoring potential [12,22,23]. A simple option to do this is the optical investigations of a Cano-Granjean wedge. Concerning the applications, the results related to the edge lasing modes (with a very low lasing threshold) should be considered as quite general. They are related not only to CLCs, but to any periodic media. Specifically, for CLCs, they reveal the direct connection of the observed jump-like phenomena in linear [6–8] and nonlinear [9,10] optics with the characteristics of the surface anchoring. These results are related also to the option of lowering the lasing threshold by the enhancement of the pumping wave absorption under conditions of the anomalously strong absorption effect in CLCs [25]. In general, CLCs should be considered as convenient model systems for the problem on the whole due to the fact that many CLC parameters are easily adjustable in experiments.

Another phenomena of a similar kind in the optics of confined CLCs, which have not been examined here, are the nonlinear optical frequency conversion [26,27] and the so-called defect modes in CLCs [14]. The corresponding effects in confine CLCs should be subjected to a further investigation because of both the value of their applications and the above-mentioned option to use CLCs as convenient model systems for the experimental investigation.

REFERENCES

[1] De Vries, H. (1951). *Acta Cryst.*, 4, 219.
[2] de Gennes, P. G. & Prost, J. (1993). *The Physics of Liquid Crystals*, Clarendon Press: Oxford.
[3] Belyakov, V. A. & Dmitrienko, V. E. (1989). Optics of chiral liquid crystals, p. 80. In: *Soviet Scientific reviews/Section A, Physics Reviews*, Khalatnikov, I. M. (Ed.), Harwood Academic Publisher, Vol. 13, 1–203.
[4] Belyakov, V. A. (1992). *Diffraction Optics of Complex Structured Periodic Media*, Springer: New York.

[5] Berreman, D. W. & Sheffer, T. J. (1970). *Phys. Rev. Lett.*, *25*, 577; *Phys. Rev.*, *11*, 1397.
[6] Zink, H. & Belyakov, V. A. (1996). *JETP Letters*, *63*, 43; *MCLC*, *265*, 445.
[7] Belyakov V. A. & Kuczynski, W. (2005). *MCLC 238*, 123.
[8] Greubel, W. (1974). *Appl. Phys. Lett.*, *25*, 5.
[9] Furukawa, T., Yamada, T., Ishikawa, K., Takezoe, H., & Fukuda, A. (1995). *Appl. Phys. B*, *60*, 485.
[10] Funamoto, K., Ozaki, M., & Yoshino, K. (2003). *Jpn. J. Appl. Phys.*, *42*, L1523.
[11] Belyakov, V. A. & Kats, E. I. (2000). *JETP*, *91*, 488.
[12] Belyakov, V. A., Stewart, I., & Osipov, M. A. (2005). *Phys. Rev. E*, *71*, 051708.
[13] Belyakov, V. A., Gevorgian, A. A., Eritsian, O. S., & Shipov, N. V. (1987). *Zh. Tekhn. Fiz.*, *57*, 1418; [Sov. Phys. Techn. Physics, *32*, 843–845, (1987) English translation].
[14] Kopp, V. I., Zhang, Z.-Q., & Genack, A. Z. (2003). *Progr. Quant. Electron.*, *27*, 369.
[15] Kogelnik, H. & Shank, C. V. (1972). *J. Appl. Phys.*, *43*, 2327.
[16] Yariv, A. & Nakamura, M. (1977). *J. Quantum Electronics*, *QE-13*, 233.
[17] Belyakov, V. A., Oswald, P., & Kats, E. I. (2003). *JETP*, *96*, 915.
[18] Belyakov, V. A. & Kats, E. I. (2001). *JETP*, *93*, 380.
[19] Zink, H. & Belyakov, V. A. (1997). *JETP*, *85*, 488.
[20] Belyakov, V. A. (2002). *JETP Letters*, *76*, 88.
[21] Belyakov, V. A. & Semenov, S. V. *Proceedings of SPIE*, Vol. 6023 (SPIE, Bellingham, WA, 2005) 6023-08.
[22] Belyakov, V. A., Stewart, I. W., & Osipov, M. A. (2004). *JETP*, *90*, 73.
[23] Belyakov, V. A., Oswald, P., & Kats, E. I. (unpublished).
[24] Belyakov, V. A., Osipov, M. A., & Stewart, I. W. (2006). *J. Phys.: Condens. Matter*, *18*, 4443.
[25] Belyakov, V. A. (2006). *MCLC*, *453*, 43.
[26] Belyakov, V. A. (1999). *JETP Lett.*, *70*, 811.
[27] Shin, K., Hoshi, H., Chung, D., Ishikawa, K., & Takezoe, H. (2002). *Optics Letters*, *27*, 128.